Evolution of the charge density wave state in Cu_xTiSe_2

M. Iavarone,[1] R. Di Capua,[1,*] X. Zhang,[1] M. Golalikhani,[1] S. A. Moore,[1] and G. Karapetrov[2]
[1]*Department of Physics, Temple University, Philadelphia, Pennsylvania 19122, USA*
[2]*Department of Physics, Drexel University, Philadelphia, Pennsylvania 19104, USA*
(Received 14 August 2011; revised manuscript received 6 March 2012; published 4 April 2012)

We present scanning tunneling microscopy and spectroscopy measurements of the charge-density wave state in $1T$-$TiSe_2$, $Cu_{0.05}TiSe_2$, and $Cu_{0.06}TiSe_2$ single crystals. Topography images at 4.2 K reveal that the charge density waves are present in all samples studied, although the amplitude of the charge modulation decreases with the Cu doping. Moreover, the chiral phase of the charge density wave is preserved also in Cu-doped samples. Tunneling spectroscopy shows that there is only a partial gap in the pure compound, with bands crossing the Fermi surface. In the Cu-doped samples, the system becomes more metallic due to the increase of the chemical potential.

DOI: 10.1103/PhysRevB.85.155103 PACS number(s): 71.45.Lr, 74.55.+v, 72.80.Ga, 73.22.Gk

I. INTRODUCTION

Transition-metal dichalcogenides are quasi-two-dimensional, highly anisotropic compounds that often show instabilities to charge density wave (CDW) formation at low temperature. The chalcogenide atoms form two parallel layers with the atoms in a hexagonal arrangement. The transition metal atoms exist in between these two layers. In the $1T$-type crystal structure, the transition metal atoms are octahedrally coordinated. In particular, $1T$-$TiSe_2$ undergoes a CDW phase transition below 200 K with a formation of a commensurate ($2a_0 \times 2a_0 \times 2c_0$) superlattice[1] that involves a small ionic displacement ($\leqslant$0.08 Å), and it is accompanied by a phonon softening.[2] Angle-resolved photoemission spectroscopy (ARPES) measurements revealed the band structure, with some of the details that still remain controversial. In the normal state, above the CDW state, $TiSe_2$ is either a semimetal[3,4] or a semiconductor[5,6] with a small indirect gap. The Se 4p valence band is at the Brillouin zone center Γ while the Ti 3d conduction band forms pockets at the Brillouin zone boundary L. In the CDW state, the Se 4p bands become backfolded. The origin of the CDW state remains still a matter of controversy up to date. The CDW transition is not likely to originate from nesting since parallel sheets of the Fermi surface were not detected by ARPES measurements. The proposed scenarios are an indirect Jahn-Teller effect,[7] an exciton insulator mechanism[8] or an exciton-phonon driven CDW.[9] Being a material with bands very close to the Fermi level, $TiSe_2$ is a unique candidate for the excitonic mechanism. Unlike many semiconductors, $TiSe_2$ has a large number of states close to E_F that makes it favorable for collective phenomena to take place. On the other hand, the small total number of carriers yields to a poorly screened Coulomb interaction, so the system is unstable to formation of excitons. However, the softening of the L_1^- mode has been observed in x-ray experiments and it might have some relevance to the CDW formation as well.[2] The discovery of superconductivity upon intercalation of Cu has further attracted the attention to this material.[10] With Cu doping it was found that the CDW transition temperature drops and the superconductivity sets in at a doping $x = 0.04$ with a highest superconducting transition temperature of 4.15 K occurring at $x = 0.08$. With a single electron in the 4s shell there is a charge transfer from the Cu to the $TiSe_2$ layers, which shifts the chemical potential and enhance the total density of states around the Fermi energy, thus facilitating superconductivity.

Scanning tunneling microscopy experiments on the undoped compound[11] revealed a domain structure CDW that has been interpreted as a sign that the CDW in $TiSe_2$ is chiral. This means that the main q vector in the CDW rotates as it goes deeper into the sample (along the c axis). This produces in each plane domains that are mirror images of each other. Although chirality is a commonly observed phenomenon in many systems chiral CDW were first reported in Ref. 11. Also, triangular shaped defect have been detected on the $TiSe_2$ surface and they have been interpreted as change in local crystal structure[12] or as Friedel oscillations that might reflect electronic properties in this material.[13]

We studied the CDW phase of $1T$-Cu_xTiSe_2 single crystals ($x = 0$, 0.05, and 0.06) with scanning tunneling microscopy and spectroscopy, and we found that the amplitude of the CDW decreases as a function of doping with clear supermodulation in all samples studied. The chiral phase is still present in doped samples, close to the critical doping at which the CDW disappears. Despite extensive studies of $TiSe_2$, tunneling spectroscopy has only been reported by using tunnel junctions[15] showing a very high value of the CDW gap in disagreement with ARPES and optical spectroscopy.[16] No tunneling spectroscopy has been reported so far for the Cu-doped samples. In this paper, we report on local tunneling spectroscopy performed at 4.2 K as a function of the doping.

II. EXPERIMENTAL DETAILS AND SAMPLE CHARACTERIZATION

Crystals were grown from Ti and Se powder by iodine vapor transport at 700 ° C.[17] X-ray diffraction pattern confirmed the crystal structure. The copper content was determined by energy dispersive x-ray microprobe analysis (EDS). Multiple regions on each crystal surface were analyzed. The EDS spectrum showed that the atomic concentration of Cu at different locations were similar. Moreover, the crystal lattice parameters measured by x-ray as well as the superconducting critical temperatures T_c were in agreement with previous reports.[18] The dc resistivity was measured by a standard four probe technique. The in-plane resistivity of the undoped

sample slightly increases by decreasing the temperature from 300 K, shows a broad hump with a maximum at about 150 K. The maximum resistance of the sample at 150 K is three times larger as that at room temperature, indicating a good stoichiometry. The resistivity at low temperature is $\approx$1 mΩ cm. For the $Cu_{0.05}TiSe_2$ and $Cu_{0.06}TiSe_2$ crystals, the in-plane resistivity is metallic with a residual resistivity ratio $\rho_{ab}(300\ \mathrm{K})/\rho_{ab}(4\ \mathrm{K}) = 4$ and 4.5 for the two samples, respectively. The resistivity just above the superconducting transition is 100 $\mu\Omega$ cm for the $Cu_{0.05}TiSe_2$ crystal and 70 $\mu\Omega$ cm for the $Cu_{0.06}TiSe_2$ crystal. The corresponding superconducting critical temperatures are $T_c = 2.0$ and 3.0 K.

Low-temperature scanning tunneling microscopy (STM) and spectroscopy (STS) have been performed at $T = 4.2$ K using a Unisoku UHV STM system, with a base pressure of 1×10^{-10} Torr. The samples were cleaved just before cooling down. We used Pt-Ir tips in all of our experiments, therefore the tunneling conductance between a normal electrode (tip) and a sample provides, in the limit of low voltages, the electronic density of states of the sample. All STM and STS measurements reported in this paper have been performed at 4.2 K and therefore the samples are in the CDW state but not in the superconducting state.

III. STM CHARACTERIZATION OF THE CDW STATE

Atomically resolved images were acquired in the constant current mode with a constant voltage between sample and tip. Figure 1(a) shows a 12.1×8.9 nm^2 STM image of pure $TiSe_2$. All surface Se atoms of the hexagonal surface layer are clearly resolved with a strong superlattice modulation $2a_0 \times 2a_0$ clearly seen in direct space.

A closer look at the amplitude of the modulation along the three directions reveals that the amplitude along the crystallographic direction $\mathbf{a_2}$ has higher intensity than that along $\mathbf{a_3}$ and $\mathbf{a_1}$, in the top region B of the topography image. The same analysis reveals instead $I_{a1} > I_{a3} > I_{a2}$ in the bottom of the image [portion A of Fig. 1(a)]. We name the phase in region A clockwise and that in region B anticlockwise, where clockwise and anticlockwise indicates the direction of increasing amplitude. These two domains cannot be superimposed on each other with simple rotational transformation, but they are mirror images of each other. This observation in agreement with previous reports[11] indicates the chiral state of the CDW in $TiSe_2$. The line profiles along the three directions in region B are reported in Fig. 1(b) while those related to the region A are reported in Fig. 1(c). The relative intensities of the modulations are $I_{a1} : I_{a2} : I_{a3} = 0.3 : 1 : 0.7$ in region B and $I_{a1} : I_{a2} : I_{a3} = 1 : 0.5 : 0.7$ in region A. These profiles have been normalized to the maximum amplitude along each direction. The profiles can slightly change from location to location especially when approaching a different domain. Therefore the relative intensity of the modulations along the three directions can slightly change depending on location and how the profiles are normalized. However, different normalizations do not affect the main result that the amplitudes of the CDW change along the three direction across the image forming chiral domains.

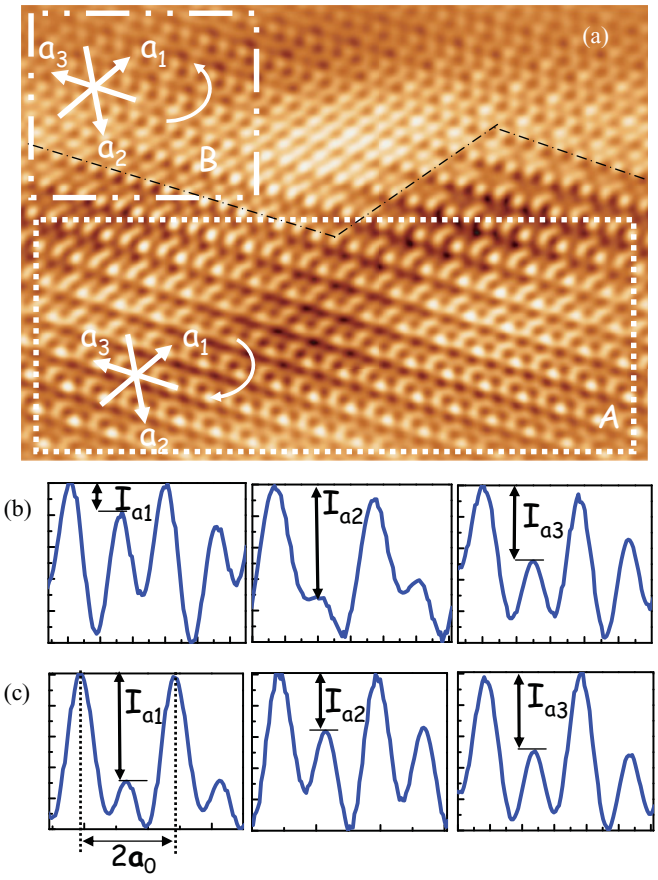

FIG. 1. (Color online) (a) 12.1×8.9 nm^2 STM topography image of pure $TiSe_2$ acquired at $T = 4.2$ K. Scanning parameters are $I = 300$ pA and $V = -0.2$ V. The dashed dark line shows the transition between two different domains. (b) Line profiles along the unit vectors $\mathbf{a_1}$, $\mathbf{a_2}$, and $\mathbf{a_3}$ in the region B of image (a). I_{ai} is the normalized amplitude of the STM corrugation along a_i. (c) Line profiles along the unit vectors $\mathbf{a_1}$, $\mathbf{a_2}$, and $\mathbf{a_3}$ in the region A of image (a).

The same conclusion can be drawn from the two-dimensional Fourier transform (2DFT) of the region A [see Fig. 2(a)] and region B [see Fig. 2(b)].[19] The 2DFT shows in both cases two sets of peaks. The outer peaks corresponds to the Bragg peaks of the Se lattice whose wavelength is a_0, the inner peaks correspond to the CDW superlattice peaks whose wavelength is $2a_0$. The three sets of CDW peaks have different intensities in the two images. The 2DFT of region A in the topography image reported in Fig. 1 shows that the CDW peaks increase in intensity clockwise with a normalized amplitude of $I_{q1} : I_{q2} : I_{q3} = 1.0 : 0.33 : 0.45$, while in the 2DFT of region B they increase in intensity anticlockwise with a normalized amplitude of $I_{q1} : I_{q2} : I_{q3} = 0.46 : 1.0 : 0.7$.

The same measurements and analysis have been performed for the $Cu_{0.05}TiSe_2$ and $Cu_{0.06}TiSe_2$ crystals. In Fig. 3(a), a 15×6.3 nm^2 STM image for $Cu_{0.05}TiSe_2$ is reported. The 2DFT of the regions A and B are shown in Figs. 3(c) and 3(d), respectively, indicating clockwise increase of the CDW amplitudes in region A and anticlockwise increase of the CDW amplitudes in region B. The normalized amplitudes of the 2DFT CDW peaks are $I_{q1} : I_{q2} : I_{q3} = 0.5 : 1.0 : 0.4$ in region A [see Fig. 3(e)] and $I_{q1} : I_{q2} : I_{q3} = 1.0 : 0.8 : 0.7$ in region

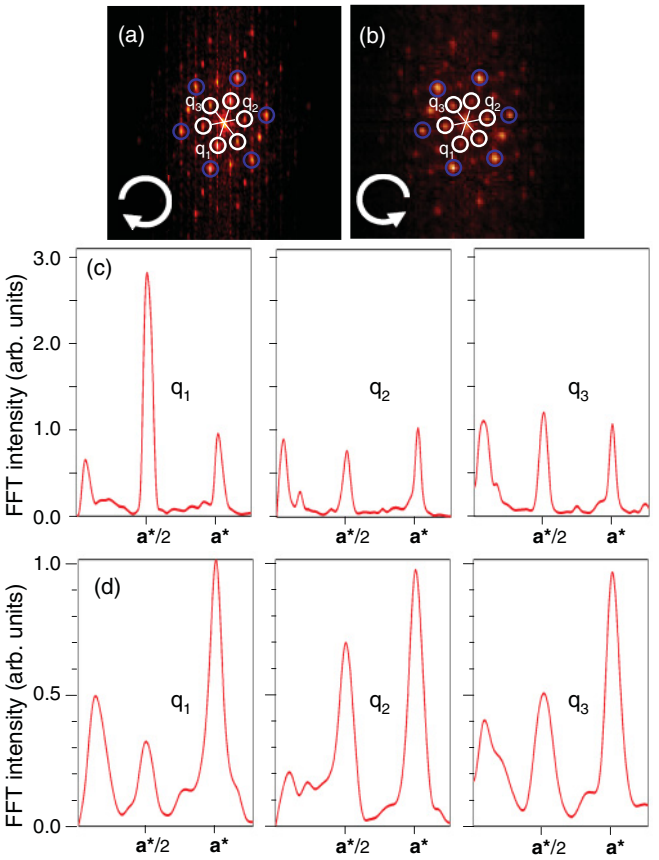

FIG. 2. (Color online) Two-dimensional Fourier transform of the region A (a) and region B (b) of the image in Fig. 1(a). Blue circles mark the Bragg peaks. The inner peaks correspond to the CDW superlattice peaks and they are marked with white circles. (c) and (d) Line profiles of the two-dimensional Fourier transform along the three q vectors: $\mathbf{q_1}$, $\mathbf{q_2}$, and $\mathbf{q_3}$, in the region A and region B, respectively.

B [see Fig. 3(f)]. In Fig. 4(a), a 20×8.4 nm^2 STM image for $Cu_{0.06}TiSe_2$ is reported. The 2DFT of the region A (in the top right corner) is reported in Fig. 4(c) while the 2DFT of region B in is reported in Fig. 4(d). The CDW peaks intensities for the two regions are shown in Figs. 4(e) and 4(f). We find a clockwise increase of the CDW amplitudes in region A and anticlockwise increase in region B. The normalized amplitudes of the 2DFT CDW peaks are $I_{q1} : I_{q2} : I_{q3} = 1.0 : 0.3 : 0.5$ in region A [see Fig. 4(e)] and $I_{q1} : I_{q2} : I_{q3} = 1.0 : 0.75 : 0.6$ in region B [see Fig. 4(f)].

The microscopic mechanism of the chiral CDW in $TiSe_2$ has been explained in terms of orbital order that introduces a phase shift between the three components of the CDW, while in the usual nonchiral state all components share the same phase.[14] The top view image obtained by STM consists of CDW modulations in the three crystallographic direction superimposed to the atomic modulations and having different intensities that form a low-symmetry structure. In pure $TiSe_2$, the CDW modulations varies on the surface between 2 and 5 Å in the three crystallographic directions and on different portion of the image. By filtering out the atom periodicity, we can visualize directly the CDW contrast. In Fig. 3(b), the CDW correlations obtained from Fig. 3(a) by filtering out the atoms are reported for the $Cu_{0.05}TiSe_2$ crystal. If the three

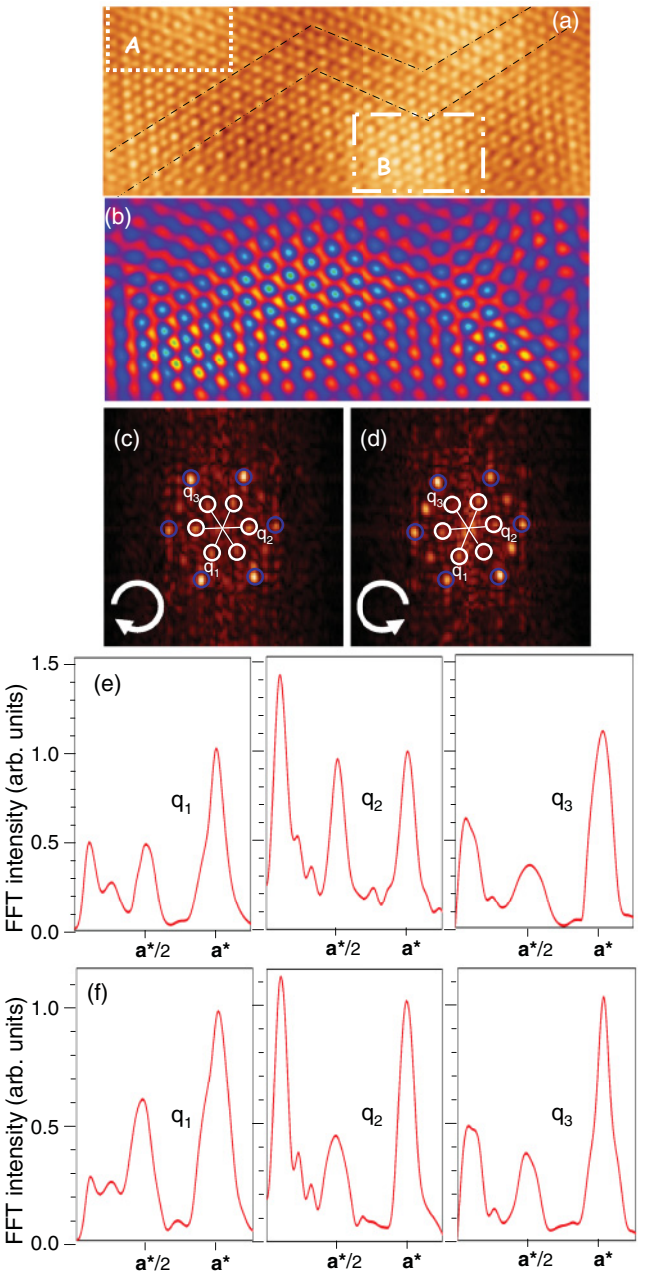

FIG. 3. (Color online) (a) 15×6.3 nm^2 STM topography image of a $Cu_{0.05}TiSe_2$ single crystal acquired at $T = 4.2$ K. Scanning parameters are $I = 300$ pA and $V = -0.2$ V. The two dark dashed lines show the transition region between two different domains. (b) CDW modulations obtained from the atomic image in Fig. 3(a). The atomic modulation has been removed by Fourier transform filtering. The color scale goes from dark blue (for CDW minima) to red (for CDW maxima). (c) and (d) Two-dimensional Fourier transform of the region A and region B shown in the image in Fig. 3(a), respectively. Blue circles mark the Bragg peaks. The inner peaks correspond to the CDW superlattice peaks and they are marked with white circles. (e) and (f) Line profiles of the two-dimensional Fourier transform along the three q vectors: $\mathbf{q_1}$, $\mathbf{q_2}$, and $\mathbf{q_3}$, in the regions A and B, respectively. The intensities increase clockwise in region A and anticlockwise in region B.

modulations intensities in the three crystallographic directions were the same, the CDW image should show hexagonal

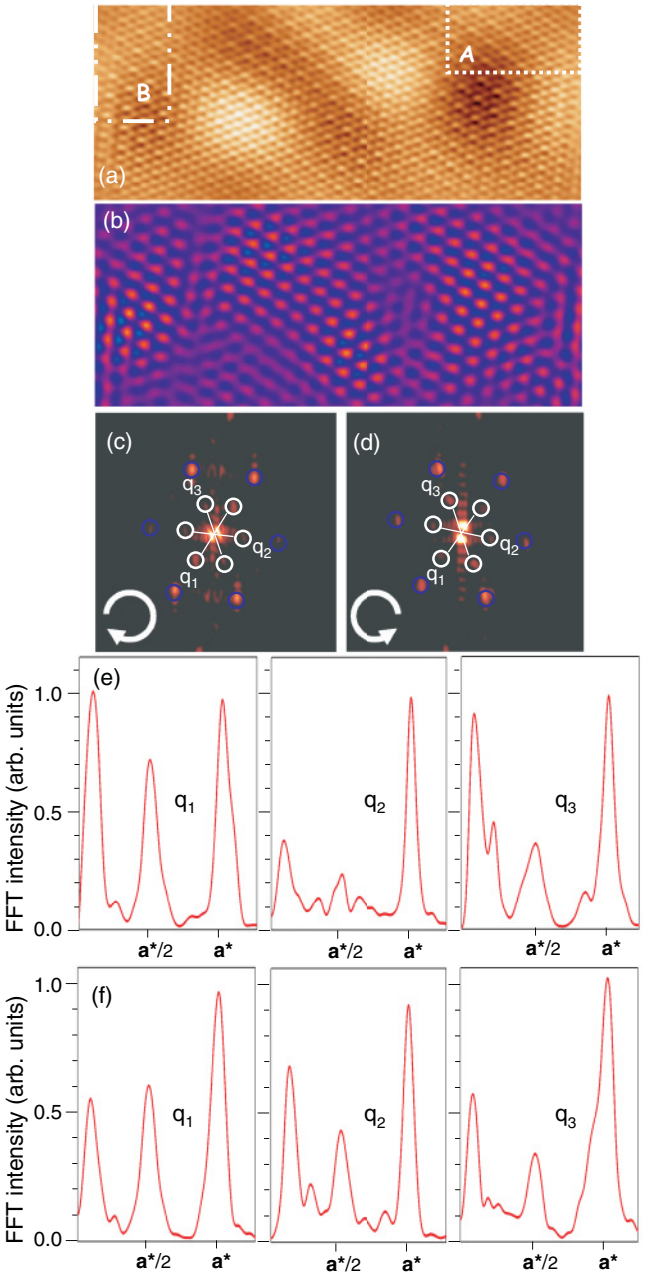

FIG. 4. (Color online) (a) 20×8.4 nm^2 STM topography image of a $Cu_{0.06}TiSe_2$ single crystal acquired at $T = 4.2$ K. Scanning parameters are $I = 300$ pA and $V = -0.2$ V. (b) CDW modulations obtained from the atomic image in Fig. 4(a). The atomic modulation has been removed by Fourier transform filtering. The color scale goes from dark blue (for CDW minima) to red (for CDW maxima). (c) and (d) Two-dimensional Fourier transform of the region A and region B shown in the image in Fig. 3(a), respectively. Blue circles mark the Bragg peaks. The inner peaks correspond to the CDW superlattice peaks and they are marked with white circles. (e) and (f) Line profiles of the two-dimensional Fourier transform along the three q vectors: $\mathbf{q_1}$, $\mathbf{q_2}$, and $\mathbf{q_3}$, in the regions A and B, respectively. The intensities increase clockwise in region A and anticlockwise in region B.

patterns of circular shaped CDW maxima. The image that we obtain reveals instead CDW maxima extended in one crystallographic direction and the shape of the maxima changes through the image. This indicates that the crystallographic directions along which the CDW modulations are maximum or minimum are changing on the surface. Circular-shaped CDW maxima are obtained in the transition regions. The CDW amplitudes for the $Cu_{0.05}TiSe_2$ crystal vary between 0.3 and 0.8 Å trough the image. In Fig. 4(b), the CDW correlations obtained from Fig. 4(a) by filtering out the atoms are reported for the $Cu_{0.06}TiSe_2$ crystal. In this case, we also find two regions A and B of opposite chirality but there is a wide region in between in which the CDW maxima form a regular hexagonal pattern with circular-shaped CDW maxima. Therefore the transition between the two types of domains of opposite chirality appears to be much larger than those observed in the pure sample and in the $Cu_{0.05}TiSe_2$. The CDW amplitudes change between 0.2 and 0.4 Å for this level of Cu doping.

Chiral-nonchiral phase transition is expected theoretically close to the CDW transition temperature and in general when the CDW state is suppressed.[14] The STM patterns observed in this study clearly show a phase difference between the three CDW components in all samples studied, therefore suggesting that the chiral CDW state is present in these samples. In general, bulk measurements such as x-ray or indirectly optical reflectometry would be needed to confirm the chiral state. However, pure $TiSe_2$ has chiral CDW as proven by other experiments.[11] Therefore our STM measurements strongly suggest that the chiral CDW state is preserved in Cu-doped $TiSe_2$ up to doping levels that are close to the critical doping at which charge density waves disappear.

IV. TUNNELING SPECTROSCOPY

Tunneling spectra have been acquired using the lock-in ac modulation technique while the I-V curves were recorded simultaneously. Good quality of the surface and atomically resolved images allow us to get reproducible spectra. Tunneling spectra are reproducible also as a function of location with some differences only in the background at higher energy but not in the features at lower energy discussed below. Representative differential conductance spectra dI/dV for $TiSe_2$, $Cu_{0.05}TiSe_2$, and $Cu_{0.06}TiSe_2$ single crystals are reported in Fig. 5. In the undoped sample the value of the zero bias conductance is nonzero indicating the presence of bands crossing the Fermi surface. This is in agreement with ARPES measurements that reveal that at low temperature the Ti $3d$ band crosses E_F twice.[4] The tunneling spectra for pure $TiSe_2$ therefore reveal a partial gap indicating that only some portions of the Fermi surface are gapped. Obtaining quantitative estimate of the gap is not straightforward when gapping involves only some portions of the Fermi surface. Two clear kinks (i.e., changes in the slope) are observed in the tunneling spectra of the undoped sample at $\varepsilon_1 \approx -153$ meV and $\varepsilon_2 \approx +1.5$ meV suggesting a partial gap of $\approx$155 meV very close to other estimates.[4,16,20] A third kink in the tunneling spectra at $\varepsilon_3 \approx -200$ meV is probably associated with the maximum of the second Se $4p$ band, as suggested by ARPES measurements. Our data seem to be in disagreement with a very high value of the gap of about 0.5 eV at 77 K reported from tunnel junction, with Al counter-electrode, measurements.[15] Although, we see in our spectra other features at higher energies like the kink at +350 meV, we do believe that these

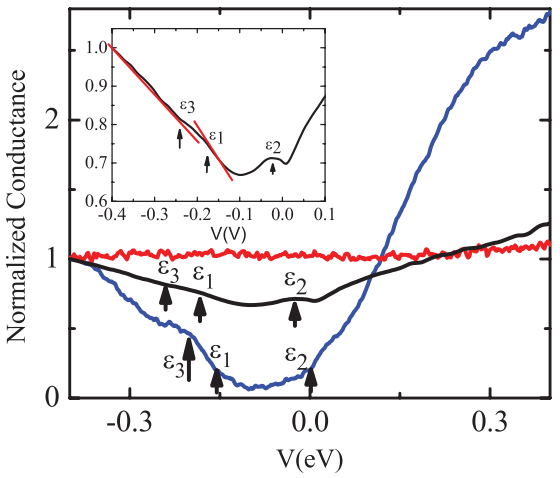

FIG. 5. (Color online) Representative conductance spectra dI/dV vs V acquired on $TiSe_2$ (blue line), $Cu_{0.05}TiSe_2$ (black line), and $Cu_{0.06}TiSe_2$ (red line) single crystals. The tunneling spectra have been acquired with the same initial parameters: $I = 50$ pA and $V = -0.5$ V, the same bias modulation amplitude $V_{mod} = 5.0$ mV (root mean square) and the same modulation frequency $f = 373$ Hz. The spectra for pure $TiSe_2$ and $Cu_{0.05}TiSe_2$ have been obtained by averaging 50 spectra, while the spectrum for $Cu_{0.06}TiSe_2$ has been obtained by averaging ten spectra taken at the same location. In the inset, it is shown in more detail the tunneling spectrum for $Cu_{0.05}TiSe_2$ close to the Fermi energy with the two changes in slope possibly associated to ε_1 and ε_2. All spectra, in the main panel as well as in the inset, have been normalized to the conductance value at $V = -0.4$ eV.

features are associated with higher-energy bands details. The total density of states shows also a high asymmetry of the tunneling spectra for extraction (negative energy) and injection of electrons (positive energy) in the undoped crystal, which is about 60% between -0.4 and $+0.4$ eV. According to band structure calculations, the Ti $3d$ bands are very close to E_F and they contribute the most to the total density of states for the unoccupied states.[21] Upon Cu doping the tunneling spectra reveal an increase of the total density of states close to E_F. In the case of $Cu_{0.05}TiSe_2$, there are two kinks (i.e., changes in slope) that are still visible and possibly can be associated to ε_1 and ε_2. These features become much weaker as shown in the inset of Fig. 5, but the changes in slope of the spectrum are still visible and above the level of noise. ARPES measurements[20] show that the Se $4p$ bands are found to weaken significantly with increasing doping. The spectra also show an increase of the total density of states and a reduction of the asymmetry between occupied and unoccupied states, which is $\approx$20% for this level of doping. With further increase of the Cu concentration the total density of states continue to increase, the asymmetry between extraction and injection of electrons is further reduced to only 9% between -0.4 and $+0.4$eV in the $Cu_{0.06}TiSe_2$ crystal. The tunneling spectra in this case are metallic and do not reveal any gap feature close to E_F. The reduced asymmetry as well as the shifting of the Se $4p$ bands are signature of the shifting of the chemical potential toward Ti $3d$ as a function of doping.

V. CONCLUSIONS

In conclusion, we report on simultaneously tunneling spectroscopy and topography on $TiSe_2$, $Cu_{0.05}TiSe_2$, and $Cu_{0.06}TiSe_2$ single crystals at 4.2 K. In STM topography, images we observe domains consistent with the chiral CDW phase already reported for the undoped sample.[11] Our measurements strongly suggest that the chiral state is preserved also in the doped crystals. The crystal Cu_xTise_2 with $x = 0.06$ is very close to the critical point where CDW order vanishes. These measurements suggest that the transition between chiral and nonchiral phase will lie very close to the CDW critical point or even at the same CDW critical point. We also observe the weakening of the CDW with an amplitude of the charge modulation that decreases as a function of Cu doping. Moreover, tunneling spectroscopy revealed a partial gap that is present only on some portions of the Fermi surface with bands crossing the Fermi level in the undoped compound. Kinks in the tunneling spectra reveal the maxima of the Se $4p$ bands. We do observe a reduced asymmetry between occupied and unoccupied states as well as an increase of total density of states upon doping.

ACKNOWLEDGMENTS

The authors would like to acknowledge very useful discussions with Jasper van Wezel and Utpal Chatterjee. This work was supported by US Department of Energy under Grant No. DE-SC0004556.

*Permanent address: Dipartimento S.pe.S., Università degli Studi del Molise, Campobasso, and CNR-SPIN, Napoli, Italy.

[1]F. J. Di Salvo, D. E. Moncton, and J. V. Waszczak, Phys. Rev. B **14**, 4321 (1976).
[2]M. Holt, P. Zschack, H. Hong, and M. Y. Chou, and T. C. Chiang, Phys. Rev. Lett. **86**, 3799 (2001).
[3]O. Anderson, R. Manzke, and M. Skibowski, Phys. Rev. Lett. **55**, 2188 (1985).
[4]Th. Pillo, J. Hayoz, H. Berger, F. Levy, L. Schlapbach, and P. Aebi, Phys. Rev. B **61**, 16213 (2000).
[5]C. H. Chen, W. Fabian, F. C. Brown, K. C. Woo, B. Davies, and B. Delong, and A. H. Thompson, Phys. Rev. B **21**, 615 (1980).
[6]T. E. Kidd, T. Miller, M. Y. Chou, and T.-C. Chiang, Phys. Rev. Lett. **88**, 226402 (2002).
[7]H. Hughes, J. Phys. C **10**, L319 (1977).
[8]J. A. Wilson and S. Mahajan, Commun. Phys. **2**, 23 (1977).
[9]J. van Wezel and P. Nahai-Williamson, and Siddarth S. Saxena, Phys. Rev. B **81**, 165109 (2010).
[10]E. Morosan, H. W. Zandbergen, B. S. Dennis, J. W. G. Bos, Y. Onose, T. Klimczuk, A. P. Ramirez, N. P. Ong, and R. J. Cava, Nat. Phys. **2**, 544 (2006).
[11]J. Ishioka, Y. H. Liu, K. Shimatake, T. Kurosawa, K. Ichimura, Y. Toda, and M. Oda, and S. Tanda, Phys. Rev. Lett. **105**, 176401 (2010).

[12]A. S. Razinkin, A. N. Enyashin, T. V. Kuznetsova, A. N. Titov, M. V. Kuznetsov, and A. L. Ivanovskii, J. Struct. Chem. **51**, 737 (2010).
[13]J. Ishioka, T. Fujii, K. Katono, K. Ichimura, T. Kurosawa, M. Oda, and S. Tanda, Phys. Rev. B **84**, 245125 (2011).
[14]J. van Wezel, Europhys. Lett. **96**, 67011 (2011).
[15]Y. Miyahara, H. Bando, and H. Ozaki, J. Phys.: Condens. Matter **7**, 2553 (1995).
[16]G. Li, W. Z. Hu, D. Qian, D. Hsieh, M. Z. Hasan, E. Morosan, R. J. Cava, and N. L. Wang, Phys. Rev. Lett. **99**, 027404 (2007).
[17]C. S. Oglesby, E. Bucher, C. Kloc, and H. Hohl, J. Cryst. Growth **137**, 289 (1994).
[18]G. Wu, H. Yang, L. Zhao, X. Luo, T. Wu, G. Wang, and X. Chen, Phys. Rev. B **76**, 024513 (2007).
[19]Two-dimensional Fourier transform of STM topography images were performed by WSXM5.0 SPM analysis software. I. Horcas, R. Fernandez, J. M. Gomez-Rodriguez, J. Colchero, J. Gomez-Herrero, and A. M. Baro, Rev. Sci. Instrum. **78**, 013705 (2007).
[20]J. F. Zhao, H. W. Ou, G. Wu, B. P. Xie, Y. Zhang, D. W. Shen, J. Wei, L. X. Yang, J. K. Dong, M. Arita, H. Namatame, M. Taniguchi, X. H. Chen, and D. L. Feng, Phys. Rev. Lett. **99**, 146401 (2007).
[21]R. A. Jishi and H. M. Alyahyaei, Phys. Rev. B **78**, 144516 (2008).